Surface plasmon resonance enhanced photoconductivity in Cu nanoparticle films

Ki Youl Yang,[1] Kyung Cheol Choi[1,*] Il-Suk Kang[2], and Chi Won Ahn[2,3]

[1]*Department of Electrical Engineering, KAIST, Daejeon 305-701, Republic of Korea*
[2] *National Nanofab Center, Daejeon 305-701, Republic of Korea*
[3]*cwahn@nnfc.re.kr*
**kyungcc@ee.kaist.ac.kr*

Abstract: We describe an all-electrical plasmon detection based on the near field coupling between plasmons and percolating electrons. It is the technique to electrically detect the local field enhancement from randomly distributed Cu nanoparticles coupled to a plasmon resonance. In addition, we revealed that plasmon-sensitivity is maximized at the percolation threshold, the minimum Cu particle surface coverage which can make the percolation path through the particles. Our detectors have a simple structure for easy fabrication and a high level of sensitivity to plasmon resonance.

OCIS codes: (230.2090) Electro-optical devices, (240.6680) Surface plasmons, (260.5150) Photoconductivity, (280.4788) Optical sensing and sensors, (310.6628) Subwavelength structures, nanostructures

References and links

1. M. E. Franke, T. J. Koplin, U. Simon;,"Metal and metal oxide nanoparticles in chemiresistors: does the nanoscale matter?" Small **2**(1), 36–50 (2006).
2. S. J. van der Molen, J. Liao, T. Kudernac, J. S. Agustsson, L. Bernard, M. Calame, B. J. van Wees, B. L. Feringa, and C. Schönenberger, "Light-controlled conductance switching of ordered metal-molecule-metal devices," Nano Lett. **9**(1), 76–80 (2009).
3. T. Vossmeyer, B. Guse, I. Besnard, R. E. Bauer, K. Müllen, and A. Yasuda, "Gold Nanoparticle/Polyphenylene Dendrimer Composite Films: Preparation and Vapor-Sensing Properties," Adv. Mater. **14**(3), 238–242 (2002).
4. N. Krasteva, I. Besnard, B. Guse, R. E. Bauer, K. Mullen, A. Yasuda, and T. Vossmeyer, "Self-Assembled Gold Nanoparticle/Dendrimer Composite Films for Vapor Sensing Applications," Nano Lett. **2**(5), 551–555 (2002).
5. P. Zhou, G. J. You, Y. G. Li, T. Han, J. Li, S. Y. Wang, L. Y. Chen, Y. Liu, and S. X. Qian, "Linear and ultrafast nonlinear optical response of Ag:Bi_2O_3 composite films," Appl. Phys. Lett. **83**(19), 3876–3878 (2003).
6. Y. Hamanaka, K. Fukuta, A. Nakamura, L. M. Liz-Marzan, and P. Mulvaney, "Enhancement of third-order nonlinear optical susceptibilities in silica-capped Au nanoparticle films with very high concentrations," Appl. Phys. Lett. **84**(24), 4938–4940 (2004).
7. R. Parthasarathy, X.-M. Lin, and H. M. Jaeger, "Electronic Transport in Metal Nanocrystal Arrays: The Effect of Structural Disorder on Scaling Behavior," Phys. Rev. Lett. **87**(18), 186807 (2001).
8. M.-S. Hu, H.-L. Chen, C.-H. Shen, L.-S. Hong, B.-R. Huang, K.-H. Chen, and L.-C. Chen, "Photosensitive gold-nanoparticle-embedded dielectric nanowires," Nat. Mater. **5**(2), 102–106 (2006).
9. R. del Coso, J. Requejo-Isidro, J. Solis, J. Gonzalo, and C. N. Afonso, "Third order nonlinear optical susceptibility of Cu:Al_2O_3 nanocomposites: From spherical nanoparticles to the percolation threshold," J. Appl. Phys. **95**(5), 2755–2762 (2004).
10. M. A. Mangold, C. Weiss, M. Calame, and A. W. Holleitner, "Surface plasmon enhanced photoconductance of gold nanoparticle arrays with incorporated alkane linkers," Appl. Phys. Lett. **94**(16), 161104 (2009).
11. S. Y. Xu, J. Xu, and M. L. Tian, "A low cost platform for linking transport properties to the structure of nanomaterials," Nanotechnology **17**(5), 1470–1475 (2006).
12. E.-K. Jeon, H. Seo, C. W. Ahn, H. Seong, H. J. Choi, J.-J. Kim, K.-J. Kong, G. Buh, H. Chang, and J.-O. Lee, "Resolving microscopic interfaces in $Si_{(1-x)}Ge_{(x)}$ alloy nanowire devices," Nanotechnology **20**(11), 115708 (2009).
13. S. Kirkpatrick, "Percolation and Conduction," Rev. Mod. Phys. **45**(4), 574–588 (1973).
14. C. Pennetta, L. Reggiani, and G. Trefan, "Scaling and universality in electrical failure of thin films," Phys. Rev. Lett. **84**(21), 5006–5009 (2000).
15. C. Pennetta, G. Trefan, and L. Reggiani, "Scaling law of resistance fluctuations in stationary random resistor networks," Phys. Rev. Lett. **85**(24), 5238–5241 (2000).
16. D.-K. Kim, K. Kerman, M. Saito, R. R. Sathuluri, T. Endo, S. Yamamura, Y.-S. Kwon, and E. Tamiya, "Label-free DNA biosensor based on localized surface plasmon resonance coupled with interferometry," Anal. Chem. **79**(5), 1855–1864 (2007).

#129778 - $15.00 USD Received 8 Jun 2010; revised 8 Jul 2010; accepted 8 Jul 2010; published 20 Jul 2010

17. B. P. Rand, P. Peumans, and S. R. Forrest, "Long-range absorption enhancement in organic tandem thin-film solar cells containing silver nanoclusters," J. Appl. Phys. **96**(12), 7519–7526 (2004).
18. K. Y. Yang, K. C. Choi, and C. W. Ahn, "Surface plasmon-enhanced spontaneous emission rate in an organic light-emitting device structure: Cathode structure for plasmonic application," Appl. Phys. Lett. **94**(17), 173301 (2009).
19. K. Y. Yang, K. C. Choi, and C. W. Ahn, "Surface plasmon-enhanced energy transfer in an organic light-emitting device structure," Opt. Express **17**(14), 11495–11504 (2009).
20. A. Kiesow, J. E. Morris, C. Radehaus, and A. Heilmann, "Switching behavior of plasma polymer films containing silver nanoparticles," J. Appl. Phys. **94**(10), 6988–6990 (2003).
21. V. K. S. Shante, and S. Kirkpatrick, "An introduction to percolation theory," Adv. Phys. **20**(85), 325–357 (1971).
22. U. Kreibig, and M. Vollmer, *Optical Properties of Metal Clusters* (Springer, Berlin, 1995).
23. S. A. Maier, *Plasmonics: Fundamentals and applications* (Springer, New York, 2007).
24. R. D. Fedorovich, A. G. Naumovets, and P. M. Tomchuk, "Electron and light emission from island metal films and generation of hot electrons in nanoparticles," Phys. Rep. **328**(2-3), 73–179 (2000).
25. C. A. Neugebauer, and M. B. Webb, "Electrical Conduction Mechanism in Ultrathin, Evaporated Metal Films," J. Appl. Phys. **33**(1), 74–82 (1962).
26. P. Banerjee, D. Conklin, S. Nanayakkara, T.-H. Park, M. J. Therien, and D. A. Bonnell, "Plasmon-induced electrical conduction in molecular devices," ACS Nano **4**(2), 1019–1025 (2010).

1. Introduction

Nanoparticle-incorporated devices have potential on practical applications in ultrafast optical switches and semiconductor-nanoparticle-based chemiresistors those are sensitive to incident photon energy or atmosphere gas environments [1–4]. Metal nanoparticle-dielectric composites show enhanced third-order optical susceptibilities, which strongly depend on the energy of the surface plasmon resonance (SPR), and the ultrafast optical response of metal-dielectric nanocomposites is involved in optical nonlinearity [5, 6]. Thus, the types of metal nanocomposites that are prepared in a thin film or bulk substrate have considerable potential for nano-scale integrated optics below the diffraction limit of light. In addition, the sensitive conductivity of semiconductor-nanoparticle-based chemiresistors is based on a shift in the equilibrium state of surface oxygen, which in turn depends on the presence of a target gas [3, 4]. These chemiresistors consist of metal-oxide nanoparticles packed between two electrodes. Furthermore, photo-sensitive molecules can be a switchable bridge between neighboring nanoparticles [2]. Several fabrication methods are used to prepare nanoparticle-embedded devices: namely spin-casting [7], metal-dielectric co-sputtering [5], hybrid nanowire synthesis [8], pulse laser deposition [9], and a combination of a self-assembly process and a microcontact printing technique [10].

Nanoparticle-incorporated device have diverse functional merits. Photonic researchers have extensively studied the idiosyncratic features of metal-dielectric nanocomposites near percolation because of their potential applications as an active material in nonlinear optical devices. Researchers have also observed that third-order optical susceptibilities depend on the percolation threshold in Au:SiO_2 and Cu:Al_2O_3 composites [5, 9] and that a nonlinear optical response at the SPR is greatly enhanced. Third-order optical nonlinearity, which is measured by a short pulse laser, is explained in terms of the local field enhancement that arises from the SPR of metal nanoclusters near the percolation threshold. In addition, Hu et al. [8] observed that the photo-sensitive resistivity of a metal-oxide-metal junction is caused by the hot electron generation induced by the decay of SPPs. Here, we demonstrate that the electrical conductivity of metal nanoparticles near the percolation threshold is effectively enhanced as a result of the augmented nonlinearity optical response induced by the enhanced local field in the Cu nanoparticles that are deposited on the Si_3N_4 substrate by means of an inert-gas condensation method.

2. Sample preparation

In order to prepare the Cu nanoparticle-embedded device, we deposited a 50-nm-thick film of Si_3N_4 and a 100-nm-thick film of Au on a Si wafer, subsequently. The 100-nm-thick-Au electrodes were patterned a 5 μm horizontal gap between the electrodes by means of photo-

#129778 - $15.00 USD Received 8 Jun 2010; revised 8 Jul 2010; accepted 8 Jul 2010; published 20 Jul 2010

lithography. And then, we back-etched away 120 μm × 120 μm segment of back side Si wafer to leave a freestanding Si_3N_4 membrane for TEM imaging [11, 12].

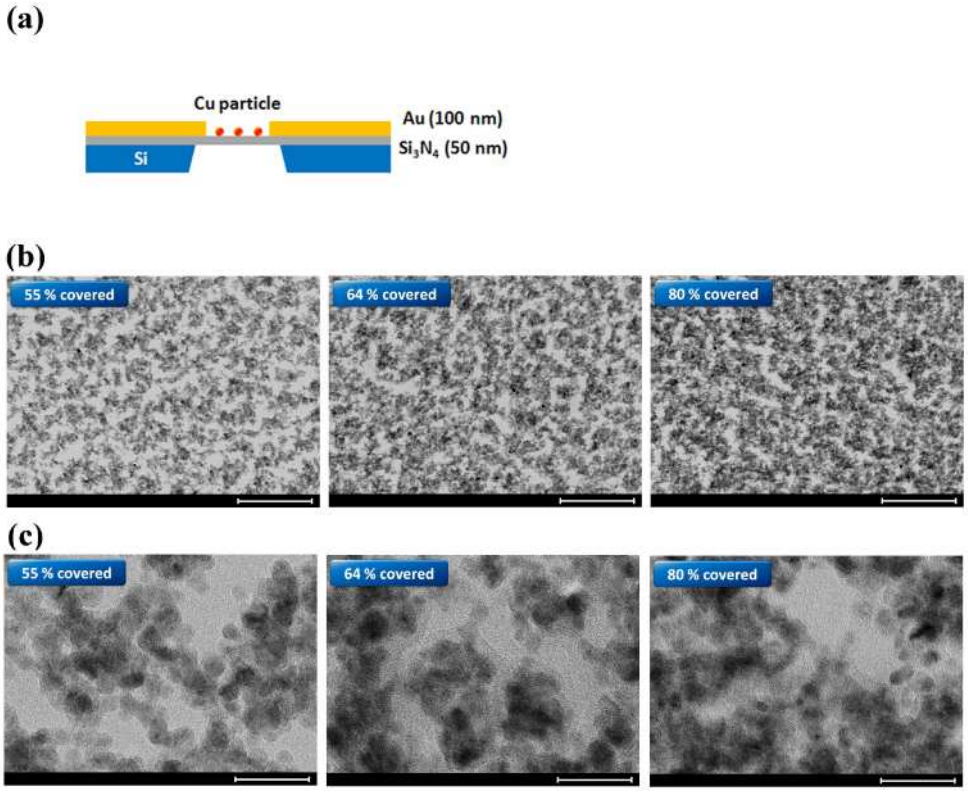

Fig. 1. (a) Device structure: the Cu nanoparticle layer is deposited on a substrate with in-plane Au electrodes. (b) TEM images of randomly deposited Cu nanoparticles, showing some voids and an absence of order; the images from left to right are samples with a surface coverage of 55%, 64%, and 80%; all scale bars=200 nm. (c) TEM images (high resolution) of randomly deposited Cu nanoparticles, showing irregular spacing between particles; some particles are arranged closely together in a range of 3 nm to 5 nm; others are spaced from each other at a distance of more than 10 nm; all scale bars=30 nm in length.

Figure 1a shows Cu nanoparticles randomly deposited on a (100) Si substrate coated with a 50 nm layer of amorphous Si_3N_4 by means of the inert gas condensation method. An inert gas condensation method is subsequently used to deposit the size-controlled metal nanoparticles on the prepared sample. Cu seed particles are sputtered from a target plane by means of DC magnetron power. Argon gas flows into the aggregation zone for the growth of metal nanoparticles. We then determine the size of the metal nanoparticles by controlling the length of the aggregation zone. After the growth of metal nanoparticles, the particles move from the aggregation zone into sample plane in an ultra-high vacuum chamber of less than 10^{-4} Torr. The resonance peak of the Cu particles used in this study is near the wavelength range of 700 nm to 800 nm. Hence, spectroscopy can more easily detect changes in the spectrum of Cu particles than in the spectra of Ag and Au particles [10].

Figure 1b shows an overview of the transmission electron microscopy (TEM) images of Cu nanoparticle deposited samples in which 55%, 64%, and 80% of the surface is covered. While the cluster deposition time increases, cluster size remains constant because the size is controlled solely by the length of the aggregation zone. Thus, the deposition time is controllable variable for the surface coverage of metal clusters deposited on the Si_3N_4 membrane. As shown in high-resolution TEM images of each sample (Fig. 1c), the metal clusters are arranged in a non-uniform manner. Some particles are arranged very closely

#129778 - $15.00 USD Received 8 Jun 2010; revised 8 Jul 2010; accepted 8 Jul 2010; published 20 Jul 2010

together, within a distance of 3 nm to 5 nm; others are arranged more than 10 nm from each other. The non-uniformity of the nanoparticle distribution causes a failure of electron conduction along the nanoparticle percolation paths. While the presence of air barrier between particles disturbs electron conduction through the metal-oxide-metal junction, electrons can overcome the inter-particle potential barrier via activated tunneling; and the conductivity of particle film decreases, if the tunneling probability is lower [13–15].

3. Experiments

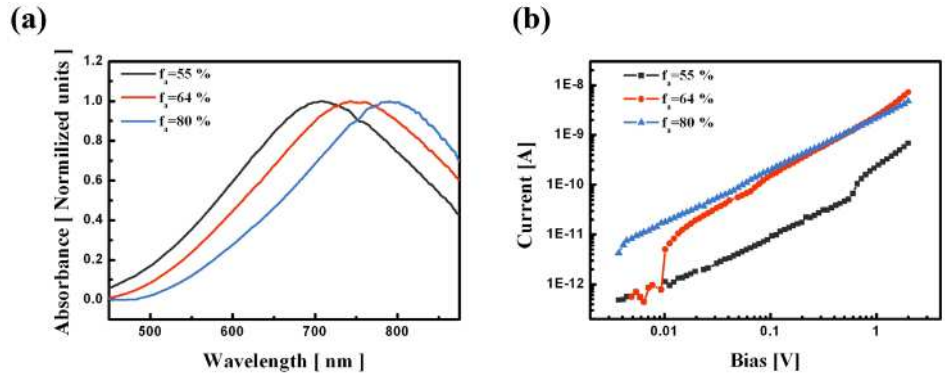

Fig. 2. (a) LSPR measurement results from samples with a surface coverage of 55%, 64%, and 80%; each samples has a different resonance peak (55%: 706 nm; 64%: 743 nm; 80%: 789 nm). (b) I-V characteristics of samples with a surface coverage of 55%, 64%, and 80%; the plot of f_a= 64% shows a jump of about one order of magnitude (for the percolation threshold).

To observe the localized SP effect of a randomly distributed metal cluster array, we investigated the localized SPR (LSPR) measurement [16]. For the plasmon resonance measurement, we prepared an LSPR system (Ocean optics Inc., USA), equipped with a tungsten halogen light source (LS-1, 360 nm to 2000 nm), a spectrometer (USB4000 UV-visible, 250 nm to 1100 nm), and an optical fiber probe bundle (R-400-7 UV-visible, 250 nm to 850 nm). The white light that emerged from the optical fiber bundle was vertically incident upon the device plane. The reflected light was coupled with the detection probe in the same bundle and analyzed with aid of a spectrophotometer. Figure 2a shows normalized measurement results of the LSPR peaks of the samples. When the ratio of the surface covered increases, the SP peak is red-shifted due to a narrowing of the space between particles [17–19]. The SP peak wavelengths for the samples with a surface coverage of 55%, 64%, and 80% are 706 nm, 743 nm, and 789 nm, respectively.

Figure 2b shows that the diagram clearly distinguishes three main structural types in terms of I-V characteristics [20]. Although Ohm's law is followed if the characteristics of f_a (which is defined as the area covered by the Cu and film) are greater than or less than 64%, the plot of f_a= 64% shows an abrupt increase in current about one order of magnitude, which is threshold of switching behavior. We confirmed that a jump of current is reversible response distinguishing from oxide breakdown, and the value of f_a= 64% is based on the threshold of the in situ measured conductance during nanoparticle deposition. In a continuum percolation model, it has been introduced that macroscopic flow through the system becomes possible and there is a completed path through allowed area consists of identical circles permitted to overlap with randomly distributed centers, at the threshold [13, 21]. The Cu particle distribution with f_a= 64% is characterized as a percolation threshold, and this value nearly corresponds to theoretical prediction of a continuum percolation model [21].

#129778 - $15.00 USD Received 8 Jun 2010; revised 8 Jul 2010; accepted 8 Jul 2010; published 20 Jul 2010

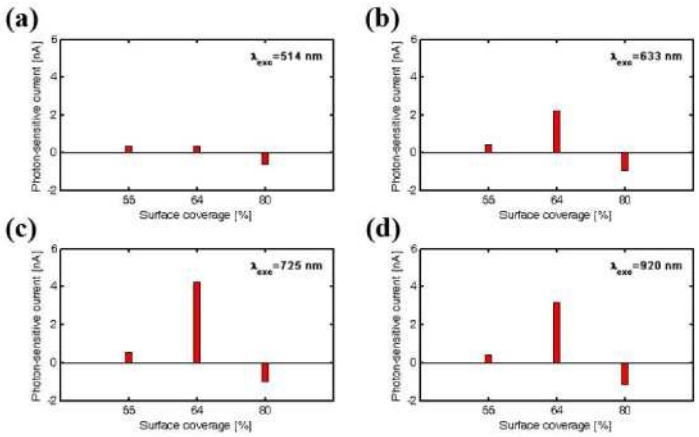

Fig. 3. Photon-sensitive current from samples of different surface coverage, varying wavelengths of illuminated laser. (a, λ_{exc}= 514 nm. b, λ_{exc}= 633 nm. c, λ_{exc}= 725 nm. d, λ_{exc}= 920 nm.) As confirmed from Fig. 2, only the sample of f_a= 64% meets at the percolation threshold condition. Every electrical properties were measured under the same bias of 2 V.

Figure 3 shows the photon-sensitive current dependence on the surface coverage of nanoparticles. Photon-enhanced currents were measured from samples which have different surface coverage of metal nanoparticles with varying the wavelengths of illuminated light source. To produce photon excitation in the sample, we placed the cell in a confocal microscope LSM510 META NLO system (Carl Zeiss, USA) for illumination with He/ Ne (discrete wavelengths of 513 nm, 543 nm, and 633 nm) and CO2 (continuous wavelengths of 710 nm to 960 nm) laser. In this experiment, we use 1 mW of laser power and an incident area of 2000 μm^2. The electron conduction features are measured in a two-point arrangement with an Agilent 4135C source-measure unit (Agilent Tech., USA). As confirmed from Fig. 3, it is obvious that percolation current is enhanced only in the sample at the percolation threshold f_a= 64%, while different conditions of nanoparticle coverage could not show both enhanced percolation current and current enhancement ratio dependence on the incidence laser wavelength at all. According to Zhou et al. [5], a nonlinear optical response in metal nanocomposites is maximized near the percolation threshold due to the photon-induced local field enhancement. When Cu nanoparticles get connected at an excessive concentration over the percolation threshold, the local field is averaged out and the enhancement effect is consequently reduced, though the local field enhancement effect is proportional to the concentration of metal nanoparticles. Thus, our observation and theoretical analysis of the plasmon-enhanced effect on the electron percolation is focused on the percolation threshold.

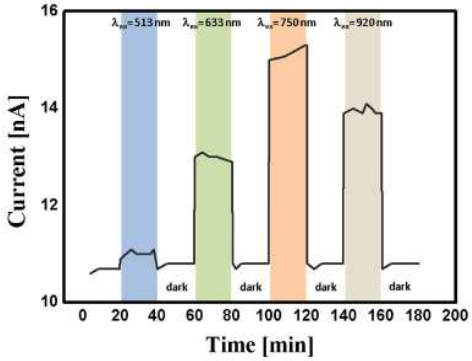

Fig. 4. The room temperature percolation current response as a function of time to light illumination for nanoparticle-embedded devices. The shaded regions (513-nm: 20 min to 40 min, 633-nm: 60 min to 80 min, 750-nm: 100 min to 120 min, 920-nm: 140 min to 160 min) and the unshaded regions mark the periods when the light is off.

#129778 - $15.00 USD Received 8 Jun 2010; revised 8 Jul 2010; accepted 8 Jul 2010; published 20 Jul 2010

Figure 4 shows the room-temperature current sensing of a Cu nanoparticle-incorporated network as a function of time to light illumination. This measurement is demonstrating device stability from oxidization and illuminated thermal damage, and we followed previous experimental methods of other groups [2, 8]. The experiment was carried out as follows: A sample embedding Cu nanoparticles is electrically connected in the ambient atmosphere of a dark room. At t = 0, we start taking measurements of the completely blocked (dark state) light source. To measure the percolation current of the Cu nanoparticles-embedded sample, we set the voltage bias between the electrodes to 2.0 V, with a relatively high percolation bias. At t = 20 min, we apply a He/ Ne laser with a 513-nm-wavelength. Immediately, a steep current increase is observed, fully consistent with plasmonic off to on conversion: because the third-order nonlinearity at the 513 nm wavelength is less than the corresponding value at other wavelengths. After 20 min of 513 nm visible light illumination, we turn to the dark state again and repeat the experiment with different illumination laser wavelengths. We alternate the dark and different wavelengths of visible IR illumination three more times, as indicated by the colored bar. From Fig. 4, we can reveal that air-exposed device is stable over 3 hours: it does not show serious current fluctuation, which came from oxidization or thermal damages of Cu nanoparticle, at all.

4. Theoretical analysis

In this work, we used the Drude-Lorentz-Sommerfeld model for modeling the optical properties of metal nanoparticles [22, 23]. This modeling is considering the electron mean free path reduction, which came from the collisions of conduction electrons with the metal particle surface. The dielectric function of Cu nanoparticle is given by

$$\varepsilon(\omega, R) = \varepsilon_{bulk}(\omega) + \omega_p^{\,2}\left(\frac{1}{\omega^2 + i\omega\Gamma_\infty} - \frac{1}{\omega^2 + i\omega\Gamma(R)}\right), \qquad (1)$$

where the cluster-radius-dependent relaxation constant $\Gamma(R) = \Gamma_\infty + Av_F / R$, the bulk relaxation term is $\Gamma_\infty = v_F / l$, v_F is the Fermi velocity, A is a dimensionless parameter, R is the radius of metal nanoparticle, and ω_p is the plasma frequency in the metallic bulk. In this work, we used the Drude-Lorentz-Sommerfeld model for describing the dielectric constants of the Cu nanoparticles, and these calculation results were used in the finite difference time domain (FDTD) simulation as the basic material properties.

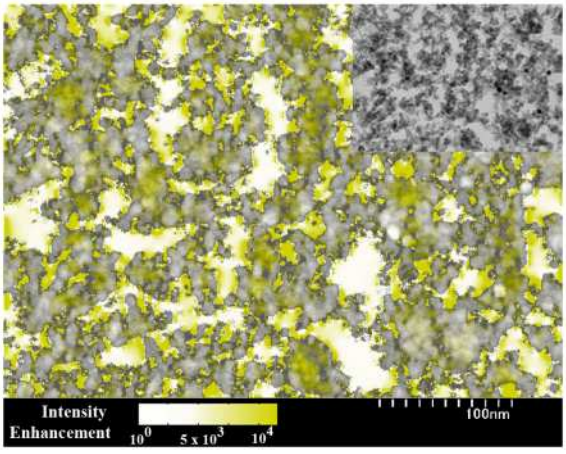

Fig. 5. Calculated electric field intensity enhancement in the plane of the deposited nanoparticles (64% coverage sample). The local field intensity enhancement is depicted in the TEM image, shown in the inset of Fig. 5, using the linear color bar.

#129778 - $15.00 USD Received 8 Jun 2010; revised 8 Jul 2010; accepted 8 Jul 2010; published 20 Jul 2010

The 3-D FDTD calculation results (64% coverage sample) are shown in Fig. 5. We use the plane wave source which propagates into the perpendicular direction with regard to the surface of nanoparticle layer, and 0.25 μm^2 of the simulated area is sufficient to be representative, because the minimum number of simulated particles (55% case) is greater than 10^4 which corresponds to larger percolation network than other groups [7, 14, 15]. The spatial distribution of the near field is plotted on the TEM image for when the wavelength of illuminated light is equivalent to that of the SP peak (λ_{sp}=743 nm): the Cu nanoparticles are indicated by gray-colored image, and the intensity enhancement is indicated by the yellow-colored bar. The spatial function of field intensity enhancement is calculated from the ratio between the local electric field intensity at the specific location and the lowest electric field intensity through the overall simulation region, and intensity enhancement is expressed by linear color bar. As shown in the near-field distribution, the field intensity is strongly enhanced near conciliated particles but weak near the distant particles. Thus, the results of the FDTD calculation confirm that SPR occurs in metal nanoparticles and that the intensity enhancement is strong through the particle percolation path.

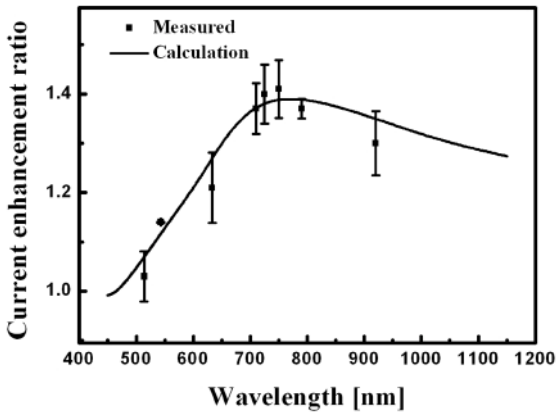

Fig. 6. The data include the measured current enhancement ratio (where the dots indicate a 95-% confidence interval error bar) and the calculated current enhancement ratio (represented by line). The horizontal axis (wavelength) means the wavelength of the illuminated light.

Following R. D. Fedorovich et al [10, 24], we attribute the non-ohmic current-voltage characteristics to the activation energy change in the ascending field between particles. Furthermore, the conductivity at the room temperature shows a simply activated behavior that corresponds with the following Arrhenius-like tunneling model [1, 25]:

$$\sigma \approx \exp(\frac{-E_A}{k_B T}) \tag{2}$$

where E_A is the activation energy for the charge transport, and $k_B T$ is the thermal energy. Because the conductivity also depends on E_A, we deduce that the conductivity of a metal nanoparticle array depends on the field between the particles. Figure 6 demonstrates the current enhancement ratio as a function of the illumination laser wavelengths. In addition, the calculation results, which are estimated from the 64% coverage sample FDTD results (Fig. 5), are depicted. All the measured dots indicate a 95% confidence interval error bar, and different sizes of them came from the different stability of illuminated light source. Because the reduction of activation energies at different wavelengths of light illumination is linearly added to that in a dark state, the photon-sensitive conductance term acts as a multiplied constant. That is,

$$\sigma \approx \exp[\frac{-(E_A - \alpha E_{loc})}{k_B T}] = \exp(\frac{-E_A}{k_B T})\exp(\frac{\alpha E_{loc}}{k_B T}), \tag{3}$$

#129778 - $15.00 USD Received 8 Jun 2010; revised 8 Jul 2010; accepted 8 Jul 2010; published 20 Jul 2010

where E_{loc} is the average intensity of surface plasmon-enhanced local field integrated over a path and α is the effective coefficient. The SP-amplified nearfield reduces the activation energy and consequently causes an exponential increase in the electron conductivity.

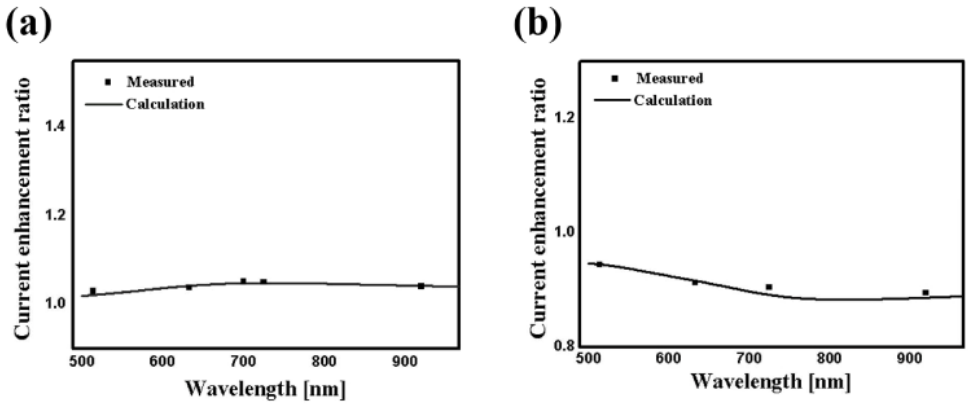

Fig. 7. (a) 55% coverage sample, measured current enhancement ratio and calculated value as a function of wavelengths to light illumination, (b) 80% coverage sampe, measured and calculated current enhancement ratio.

Contrast with the result of the 64% coverage sample, the 55% and 80% coverage sample do not show sensitive photoresponse, and the 80% coverage sample even show negative sign of photocurrent, as shown in Fig. 3. In cases of the 55% and 64% coverage samples, the electron transport can be described as an activation energy model, because Arrhenius-like model is valid for the macro system evolving from an insulating regime dominated by Coulomb blockade to a semiconductor regime. Thus, photoconductivity of the 55% coverage sample can be simillarlly described with that of the 64% coverage sample, as shown in Fig. 7a. The magnitude differences between 55% and 64% coverage samples comes from each activation energy for charge carrier creation [25]. However, the 80% coverage sample cannot be modeled using an activation enery model, because the macroscopic system already has many conduction paths and it has metallic conduction property. Thus, the photocurrent of the 80% coverage sample shows negative value due to the surface plasmon-induced temperature increases, while the 55% and 64% coverage samples have the positive photocurrent [26]. Its different behavior can be simply modeled, and the results are shown in Fig. 7b.

5. Conclusion

In conclusion, we prepared films of randomly-distributed Cu nanoparticles deposited in an optically transparent Si_3N_4 plane by using an inert-gas condensation method, with varying the surface coverage from 55% to 80%. The different split conditions with regard to the electrical pre-threshold, the threshold, and the post-threshold nanocomposite coverage confirm that the nanocomposite under the percolation threshold has the most sensitive optical-electron responses. The phenomenon proves that photon-induced SPs contribute to electron transport between particles. These experimental results suggest that a Cu nanoparticle-embedded device can detect the SPR by simply monitoring the current.

Acknowledgements

This work was supported by a grant from the National Research Foundation (NRF), which is funded by the Korea government (MEST) (No. R11-2007-045-02001-0), and the NRF (No. R01-2009-000-20675-0). The authors acknowledge the help received from Dr. D. K. Kim, and Prof. T. J. Park (KAIST) for technological support. In addition the authors greatly express acknowledgment to Dr. V. Giannini, and Prof. S. A. Maier (Imperial College London) for their theoretical advice.

#129778 - $15.00 USD Received 8 Jun 2010; revised 8 Jul 2010; accepted 8 Jul 2010; published 20 Jul 2010